Sustainability in Environment
ISSN 2470-637X (Print) ISSN 2470-6388 (Online)
Vol. 11, No. 2, 2026
www.scholink.org/ojs/index.php/se

Original Paper

Refined Risk Assessment of Geological Hazards in World Natural Heritage Sites: An Empirical Analysis of the Libo-Huanjiang Karst World Natural Heritage Site

Yuping Ding[1,2], Kangning Xiong[1,2*], & Ruonan Fang[1,2]

[1] School of Karst Science, Guizhou Normal University, Guiyang, China

[2] State Engineering Technology Institute for Karst Desertification Control, Guiyang, China

Received: February 01, 2026 Accepted: March 12, 2026 Online Published: March 23, 2026

doi:10.22158/se.v12n1p108 URL: http://dx.doi.org/10.22158/se.v12n1p108

Abstract

Refined risk assessment of geological hazards is vital for disaster prevention and loss reduction. World Natural Heritage Sites are Earth's most precious natural assets, yet research on refined geological hazard risk assessment from the perspective of heritage conservation and management is scarce. Taking the Libo-Huanjiang Karst World Natural Heritage Site as the study area, this paper discusses an assessment method focusing on protecting its Outstanding Universal Value (OUV) and draws three conclusions: ① The risk pattern features local high concentration and overall low risk: extremely high-risk areas account for 2.32% (sporadic in the northwest), low-risk areas 68.29% (covering the core zone), and high/medium-risk areas concentrate in the west with developed faults and intense human activities. ② It clarifies the non-linear synergistic mechanism of susceptibility-hazard-vulnerability, with stratum lithology, distance to roads and water systems as core drivers, and low vulnerability acting as an ecological buffer. ③ It correlates risk patterns with heritage protection, verifying the overlap between high-risk areas and key karst landscapes, and defines key prevention zones. The results support risk management and heritage protection, providing a replicable reference for similar World Natural Heritage Sites globally.

Keywords

geological hazard risk assessment, refined evaluation, world natural heritage site, risk management

1. Introduction

World Natural Heritage Sites (WNHSs) are widely recognized as the most precious natural assets with Outstanding Universal Value (OUV), whose value transcends national boundaries and deserves the

common protection of all mankind (UNESCO, Operational Guidelines for the Implementation of the World Heritage Convention, 2017; Allan et al., 2017; Wang, Yang, & Du, 2014). A natural World Heritage Site must meet at least one of the four criteria. In summary, these criteria relate to natural phenomena or aesthetic importance, geology, ecosystems, or biodiversity (UNESCO, Operational Guidelines for the Implementation of the World Heritage Convention, 2017; Zhang et al., 2022; Zhang, Xiong, & Liu, 2023). Geological values include records of life evolution, important ongoing geological processes, or significant geomorphological/physiographical features; ecological and biological values encompass important ongoing ecological and biological processes of ecosystems and flora and fauna communities, natural habitats, and endangered species (UNESCO, Operational Guidelines for the Implementation of the World Heritage Convention, 2017). Aesthetic values comprise exceptional natural phenomena or areas of exceptional natural beauty and aesthetic importance. It is generally acknowledged in academic circles that the formation of aesthetic values is closely related to unique geological and geomorphological features, diverse ecosystem types, or habitats for rare and endangered species (Du & Wang, 2018; Yang, Zhang, Di, Wall, Liu, & Shao, 2010; Beza, 2010; Han, Yang, Liu, & Di, 2011). Based on their aesthetic values, World Heritage Sites cover ten major landscape types, including lakes, waterfalls, coastlines, panoramic landscapes, geology/geomorphology, deserts, mountains, forests, meteorological landscapes, and wildlife habitats. According to the regulations of the United Nations Educational, Scientific and Cultural Organization (UNESCO), World Heritage Sites (WHS) inscribed on the World Heritage List (WHL) must be supported by appropriate protection systems to ensure their integrity and authenticity.

However, geological hazards—such as earthquakes, collapses, landslides, among others—represent one of the most critical issues and have exerted adverse impacts on WNHSs (Pavlova, Makarigakis, Depret, & Jomelli, 2017; Klimeš, 2013; Chen, 2012; Parisi & Augenti, 2013). They threaten the integrity of these sites, impair their values, and also pose substantial ecological risks. By integrating open-source global risk data with risk perception information from UNESCO periodic reports, Pavlova et al. (2017) found that 60% of the sites inscribed on the World Heritage List are exposed to at least one type of geological hazard. To minimize these impacts and achieve sustainable development, refined risk assessment of geological hazards can analyze the potential and extreme adverse effects that may be triggered by geological hazards, making it a robust technical tool. Nevertheless, up to the present, few studies have attempted to establish a refined risk assessment framework for geological hazards in natural World Heritage Sites that is oriented toward the protection of heritage values. In recent decades, conceptual research on geological hazard risk has undergone a remarkable shift: from an environment-determinism-oriented, hazard-centered research perspective (Hagenlocher, Renaud, Haas, & Sebesvari, 2018), it has gradually evolved toward a political economy and political ecology perspective (Okeefe, Westgate, & Wisner, 1976; Morin, 2015; Birkmann ea al., 2017), and finally formed a holistic concept integrating disaster risk drivers associated with society, economy, politics, environment and governance (Hagenlocher, Renaud, Haas, & Sebesvari, 2018; Cheung, 2007; Alamgir

et al., 2017; Wang et al., 2018). Despite the growing complexity and diversity of geological hazard risks, the academic community commonly defines such risk as the likelihood of adverse impacts on World Heritage Sites caused by human activities and unavoidable natural events, and regards risk as the combined outcome of hazard and vulnerability(Vašíčková, Hvězdová, Kosubová, & Hofman, 2019; Serveiss, 2002; Yanes, Botero, Arrizabalaga, & Vásquez, 2018; Steen et al., 1999).

The Libo-Huanjiang Karst World Natural Heritage Site (hereinafter referred to as the Libo-Huanjiang Heritage Site) was inscribed on the World Natural Heritage List for its aesthetic values (Criterion VII) and geological and geomorphological values (Criterion VIII), and is part of the South China Karst World Heritage Serial Site. Located on the border between Guizhou and Guangxi, the heritage site features fengcong and fenglin karst as its core landforms. The subtropical humid climate and intensive karst development have jointly resulted in extremely high susceptibility to geological hazards. The regional rock-soil mass is characterized by a structure of "less soil, more rock, and interlaced rock and soil", with significant differences in the distribution of dolomite and limestone. Superimposed with fault structures and strong dissolution by groundwater, these conditions provide a geological foundation for the occurrence of geological hazards. Collapses and landslides are the dominant hazard types, and the increasing frequency of extreme rainfall has further aggravated hazard risks. In some areas, the soil erosion rate far exceeds the allowable threshold for karst regions. As an overlapping zone between World Natural Heritage and ecologically fragile areas, geological hazards not only threaten human settlement safety but also pose potential risks to the geomorphological integrity and ecosystem stability of the heritage site. It is urgent to reveal the formation mechanism and risk pattern of hazards through refined assessment. To protect its Outstanding Universal Value (OUV) from further damage by geological hazards (which impair the integrity of the heritage site and thus weaken its aesthetic and geological-geomorphological values), the Libo-Huanjiang Heritage Site is in urgent need of refined geological hazard assessment. Therefore, establishing a quantitative risk assessment system for geological hazards is of great significance for achieving the sustainable development goals of the Libo-Huanjiang Heritage Site. This paper takes the Libo-Huanjiang Heritage Site as the study area for refined geological hazard assessment, and introduces and discusses an assessment method that prioritizes World Natural Heritage conservation and focuses on heritage values. This method will enrich the research approaches for regional geological hazard risk assessment, and can simultaneously convey risk information to relevant decision-makers and stakeholders and realize risk visualization, which has practical significance for guiding regional ecosystem protection and promoting disaster risk reduction.

2. Materials and Methods

2.1 Study Area

The Libo-Huanjiang Heritage Site is situated at the junction of Libo County, Qiannan Buyi and Miao Autonomous Prefecture, Guizhou Province, and Huanjiang County, Hechi City, Guangxi Zhuang

Autonomous Region(Fig. 1). The World Heritage Site mainly includes Maolan National Nature Reserve in Guizhou, the Daqikong and Xiaoqikong scenic areas of Zhangjiang National Scenic Area, as well as Mulun National Nature Reserve in Guangxi. The karst of the Libo-Huanjiang Heritage Site satisfies two World Heritage criteria: (vii) containing exceptional natural phenomena or areas of exceptional natural beauty and aesthetic importance; (viii) being outstanding examples representing major stages of the Earth's history, including the record of life evolution, significant ongoing geological processes in the development of landforms, or significant geomorphic/physiographic features. It is the only karst area in the world that is concentrated in distribution, highly pristine, relatively stable, and represents the largest and best-preserved karst region at the same latitude on Earth. This heritage site was nominated for NWH jointly with Shilin (Yunnan) and Wulong (Chongqing), and was inscribed on the WHL by the UNESCO World Heritage Committee in June 2007. The total area of the study area is 84 575 hectares, of which 36 647 hectares belong to the heritage site and 47 928 hectares to the buffer zone (Zhang, Xiong, & Liu, 2023).

The Libo-Huanjiang Heritage Site is located in the transitional zone between the Yangtze Paraplatform and the South China Fold Belt, with extremely complex geological structures. Fault structures are well developed in the area, mainly including the Libo-Maolan Fault and the Huanjiang-Xunle Fault, which strike NNW-trending and provide a tectonic foundation for the formation of geological hazards. The strata are dominated by carbonate rocks, with dolomite and limestone distributed alternately in bands, accompanied by intense karstification. The rock-soil mass exhibits a typical structure of "less soil, more rock, and interbedded soil and rock". Carbonate rocks have low shear strength, and intensive karst development results in high porosity and fragmented structure of the rock mass, forming numerous potential unstable masses. The heritage site features great topographic relief, with 42% of the area having slopes steeper than 25°. Micro-geomorphic units such as fengcong depressions and the foot of steep cliffs are widely distributed, forming numerous stress concentration zones. The relative elevation difference of fengcong depressions is mainly 100–300 m, and the large height gap between depression bottoms and peak tops provides considerable gravitational potential energy, which creates favorable topographic conditions for collapses and landslides. The disturbance depth of rock-soil mass in some areas reaches 1–3 m, further reducing slope stability. The study area has a subtropical humid monsoon climate, with an average annual precipitation of 1300–1600 mm. About 75% of the annual rainfall occurs from May to September, accompanied by frequent extreme rainfall events. Short-duration heavy rainfall can easily trigger saturation and instability of rock-soil masses, forming a hazard triggering mechanism of "rainfall infiltration – groundwater rise – softening of rock-soil mass". Collapses and landslides are the dominant hazard types, followed by karst collapses. The density of hazard points is high in dolomite areas but relatively sparse in limestone areas. Tourism development, slope farmland reclamation and residential expansion have destroyed vegetation, altered runoff paths, lowered the hazard triggering threshold, and aggravated risks to the geomorphological integrity and ecosystem stability of the heritage site.

Therefore, as the best-preserved primeval karst forest at the same latitude across the globe, the Libo-Huanjiang Heritage Site is of great significance for research on refined geological hazard assessment in the protection of the OUV of World Natural Heritage Sites and the prevention of geological hazards, making it an ideal empirical area for carrying out refined risk assessment.

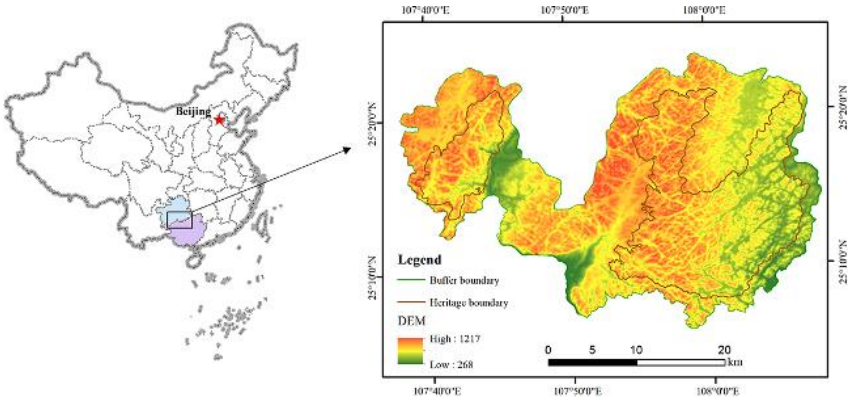

Figure 1. Location of the study area (Zhang, Xiong, & Liu, 2023)

2.2 Data Sources and Preprocessing

To assess the geological hazard risk of the Libo-Huanjiang Heritage Site, a database was established incorporating relevant documents, Digital Elevation Model (DEM) data, Landsat-8 OLI remote sensing data, precipitation data, and earthquake location data for the heritage site. All data were unified to the same geographic extent, coordinate system (WGS_1984_UTM_45N), and pixel resolution (30 × 30 meters). Relevant data for the Libo-Huanjiang Heritage Site include the boundaries of the heritage site and its buffer zone, as well as spatial data on water systems, roads, buildings, and vegetation types within the study area. The DEM data were obtained from the Geospatial Data Cloud, which contains elevation information; slope, aspect and other terrain attributes were extracted from the DEM using ArcGIS 10.2 software. Earthquake epicenter data were acquired from the China Earthquake Networks Center. Precipitation data were collected from Station 57926 (Libo County) on the China Meteorological Data Service Center of the National Meteorological Information Center.

Landsat-8 OLI images were downloaded from the official website of the United States Geological Survey (USGS) at https://glovis.usgs.gov. Satellite imagery from the growing season was selected, as it best represents the surface vegetation coverage. To convert the digital numbers of the raw images to top-of-atmosphere reflectance and reduce distortions caused by illumination and atmospheric effects, radiometric calibration and atmospheric correction were conducted using ENVI 5.3 software. The Normalized Difference Vegetation Index (NDVI) was then calculated from the corrected images using the following formula:

$$NDVI=(b_{NIR}-b_{Red})/(b_{NIR}+b_{Red}) \quad (1)$$

where b_{NIR} and b_{Red} represent the reflectance of the near-infrared band and red band of Landsat-8 OLI imagery, respectively.

2.3 Research Methods

(1) Comprehensive Index Model

The Comprehensive Index Model method (WARD et al., 2020) is a comprehensive evaluation approach. By establishing an indicator system, it performs weighted averaging or integrated calculation on multiple indicators to derive a comprehensive index, thereby reflecting the overall level or changing trend of the research object. First, several indicators that can represent the overall level are determined, and data standardization is conducted on these indicators to allow comparison on a unified basis. Then, the standardized value of each indicator is multiplied by its corresponding weight, followed by weighted averaging to compute the comprehensive index.

The calculation formula is as follows:

$$Y_i = \sum_{j=1}^{n} F_{ij} S_{ij} \tag{2}$$

where: Y_i is the comprehensive susceptibility index of the i-th grid cell; F_{ij} is the weight of the j-th indicator for the i-th grid cell; S_{ij} is the specific assigned value of the j-th indicator for the i-th grid cell.

(2) **Analytic Hierarchy Process (AHP)**

① Based on a thorough analysis and summary of the current development of geological hazards and their formative geological conditions in the study area, the hierarchical structure of the main influencing factors was clarified, and a hierarchical model was established. The model is divided into three levels: the goal layer (geological hazard susceptibility assessment), the indicator layer (influencing factors), and the scheme layer (states or intervals of each factor).

② Construction of the judgment matrix: If the weights of the factors controlling geological hazard development are determined only by qualitative judgment, the results tend to be highly subjective and unconvincing. Therefore, a judgment matrix was constructed to conduct pairwise comparisons among all influencing factors using a relative scale. This reduces the difficulty of comparing factors with different attributes and improves the accuracy of weight determination. The pairwise comparison matrix compares the relative importance of each factor in a given layer with respect to each factor in the upper layer. The relative importance between factor A and factor B is represented by the value of a_{AB}. The judgment was specifically performed using the Saaty 1–9 scale method (Table 1).

Table 1. Scale Table

Scale	Definition
1	Indicates that factor A is equally important compared to factor B.
3	Indicates that factor A is slightly more important than factor B.
5	Indicates that factor A is obviously more important than factor B.
7	Indicates that factor A is strongly more important than factor B.
9	Indicates that factor A is extremely more important than factor B.

Scale	Definition
2,4,6,8	Intermediate values between the two adjacent judgments.
Reciprocal	If the judgment comparing factor A and B is a_{AB}, then the judgment comparing factor B and A is $a_{BA}=1/a_{AB}$

Based on this, the judgment matrix T is obtained.

$$T=\begin{bmatrix} A_{11} & A_{12} & \cdots & A_{1n} \\ A_{21} & A_{22} & \cdots & A_{2n} \\ \vdots & \vdots & \vdots & \vdots \\ A_{n1} & A_{n2} & \cdots & A_{nn} \end{bmatrix} \tag{3}$$

③ Calculation of Eigenvectors

Once the judgment matrix is constructed, the eigenvectors of the matrix are calculated using the sum-product method. Through comparative calculations, the sum-product method has been verified to meet the research requirements. The specific steps are as follows:

Step 1: Normalize the elements of each column in the constructed judgment matrix.

$$A_{ij}^{'}=\frac{A_{ij}}{\sum_{i=1}^{n} A_{ij}} \cdots \ i,j=1,2,\ldots,n \tag{4}$$

Step 2: Calculate the sum of each column in the normalized judgment matrix.

$$\omega^{'}=\sum_{j=1}^{n} A_{ij} \cdots \ i=1,2,\ldots,n \tag{5}$$

Step 3: Normalize the vector $\omega=(\omega_1,\omega_2,\ldots,\omega_n)T$

$$\omega_i=\frac{\omega_i^{'}}{\sum_{i=1}^{n} \omega_i^{'}} \cdots \ i=1,2,\ldots,n \tag{6}$$

The resulting vector $\omega=(\omega_1,\omega_2,\ldots,\omega_n)$ is the approximate solution of the desired eigenvector, namely the weight values required in this study.

④ Consistency Test

Through calculating the maximum eigenvalue (λmax), consistency index (CI), and random consistency ratio (CR) of each judgment matrix, the consistency of the matrix is finally verified by the magnitude of CR, so as to judge the rationality of the obtained weight vector ω.

Step 1: Calculate the maximum eigenvalue λmax of the judgment matrix.

$$\lambda_{max}=\frac{1}{n}\sum_{i=1}^{n}\frac{A\omega}{\omega_i} \tag{7}$$

Step 2: Calculate the consistency index CI of the judgment matrix.

$$CI=\frac{\lambda_{max}-n}{n-1} \tag{8}$$

Step 3: Calculate the random consistency ratio CR.

$$CR=\frac{CI}{RI} \tag{9}$$

where RI is determined according to the empirical values in Table 2.

When the final calculated result CR < 0.1, the constructed judgment matrix can be confirmed to have satisfactory consistency.Otherwise, the judgment matrix needs to be adjusted continuously until satisfactory consistency is achieved.

Table 2. Average Random Consistency Index for AHP

n	1	2	3	4	5	6	7	8	9	10	11
RI	0.00	0.00	0.58	0.90	1.12	1.24	1.32	1.41	1.45	1.49	1.51

(3) **Hazard Index Method**

This study adopts the instability probability (i.e., hazard) of each evaluation unit in the geological hazard-prone area of the study region under different working conditions[28][29].The calculation formula is as follows:

$$H_i=(Y_i/Y_{max})P_i \tag{10}$$

Where H_i is the hazard probability of the i-th evaluation unit under a specific condition; Y_{max} is the maximum susceptibility index of the evaluation unit; and P_i is the instability probability of the i-th evaluation unit within a given time period under a specific condition.

(4) Geological Hazard Risk Assessment

Geological hazard risk assessment (CHENG et al., 2024) is based on the results of geological hazard susceptibility assessment and vulnerability assessment. Using the geological hazard risk calculation formula, geological hazards in Quanwang Town are classified into four risk levels: very high risk, high risk, medium risk, and low risk (SHU et al., 2024):

$$R_i=\sum_{j=1}^{n} H_{ij}\,E_{ij}V_{ij} \tag{11}$$

where R_i is the risk value of the i-th evaluation unit under a specific condition; H_{ij} is the geological hazard index of the j-th element at risk within the i-th evaluation unit under a specific condition; E_{ij} is the value of the j-th element at risk within the i-th evaluation unit under a specific condition; and V_{ij} is the vulnerability of the j-th element at risk within the i-th evaluation unit under a specific condition.

2.4 Evaluation Process

(1) Determination of Evaluation Units

According to the scope and accuracy of the investigation, grid units were adopted as the susceptibility evaluation units at the 1:50,000 scale in this study. Based on the collected DEM data and field survey data, spatial analysis in ArcGIS was used to assess the susceptibility of geological hazards. A grid size of 30 m × 30 m was selected for the regional geological hazard susceptibility assessment, which meets

the required evaluation accuracy. All data in the study area were rasterized using ArcGIS 10.8, yielding a total of 902,070 grid units. Data for each influencing factor were then extracted at the grid unit level.

(2) Index Selection

This study focuses on collapses, landslides, debris flows and other hazards caused by rock fragments and loose solid materials. Collapse refers to the natural downward movement of rock blocks under gravity, including free falling, rolling and sliding. Landslides are disasters in which slopes transform from a stable state to an unstable state under certain actions. Precipitation and water erosion are the main factors affecting slope instability in the Libo–Huanjiang heritage site. Debris flow is a geological phenomenon in which water-bearing soil and gravel surge rapidly down slopes, flow into river channels, and form thick muddy deposits on valley floors.

According to relevant literature (Nicu, & Romanescu, 2016; Allan,Venter, Maxwell, Bertzky, Jones, Shi, & Watson, 2017), active structures, topography and geomorphology, meteorological and hydrological conditions, as well as damage to mountain structures caused by highway construction, provide suitable internal and external dynamic conditions for the occurrence of collapses, landslides and debris flows in the Libo–Huanjiang Heritage Site. Therefore, this study evaluates hazard susceptibility, hazard, vulnerability and risk by integrating geographical environment, geological structure and other factors. Based on the analysis of the correlation between various disaster-inducing geological conditions and different types of geological hazards, as well as the correlation among their influencing factors, eight factors were finally selected as evaluation indicators for geological hazards: elevation, slope gradient, aspect, vegetation coverage, distance to water system, distance to road, distance to structure, and stratigraphic lithology. As basic topographic indicators, elevation and slope gradient are commonly used to estimate erosion intensity, surface runoff and landscape characteristics (Wang, Yao, & Deng, 2019; Xu, Yang, Zhang, Xiao, Wang, & Ouyang, 2017; Pan, 2016). Rainwater infiltration increases soil saturation, significantly reduces soil water absorption and leads to a sharp decrease in shear strength; rainwater infiltration and confluence may further trigger slope instability. Vegetation and water flow are the most important factors affecting soil erosion and slope stability. Vegetation enhances soil shear strength through a series of mechanical and hydrological effects (Wang, Yao, & Deng, 2019; Xu, Yang, Zhang, Xiao, Wang, & Ouyang, 2017; You et al., 2014). Surface vegetation coverage has been widely used as an indicator to quantify the probability of geological hazards (You et al., 2014; Ma, Lu, & Lin, 2010; Wu & Deng, 2019). Distance to rivers is a spatially simplified representation of the influence of major river flows, reflecting the role of hydrological conditions in hazard occurrence. There are many types of factors influencing geological hazard susceptibility, each containing multiple sub-factors. The selection of evaluation factors should be based on a thorough analysis of disaster-inducing geological conditions in the study area, combined with their influence degree and data extractability, so as to ensure the objectivity and accuracy of evaluation results. Based on the analysis of geological hazard development and the distribution characteristics of each factor interval, each evaluation factor was divided into sub-factors, resulting in a total of 32 sub-factors. The detailed classification of all levels of

evaluation factors and sub-factors is shown in Table 3.

According to the Technical Requirements for Geological Hazard Risk Investigation and Assessment (FXPC/ZRZY B-01), hazard assessment should adopt average rainfall, combined with the developmental characteristics of geological hazards, to carry out qualitative or quantitative hazard assessment. Therefore, based on the geological hazard susceptibility assessment, average rainfall was selected as a triggering factor for the analysis and assessment of geological hazard. Rainwater infiltration increases soil saturation, significantly reduces soil water absorption and leads to a sharp decrease in shear strength; rainwater infiltration and confluence may further trigger slope instability. Vegetation and water flow are the most important factors affecting soil erosion and slope stability. Vegetation enhances soil shear strength through a series of mechanical and hydrological effects (Wang, Yao, Deng, 2019; Xu, Yang, Zhang, Xiao, Wang, & Ouyang, 2017; You et al., 2017). The rainfall return period was calculated according to the rainfall interval distribution, and then superimposed with the geological hazard susceptibility index to obtain the geological hazard index. Finally, the geological hazard analysis and assessment were carried out.

The evaluation subject of geological hazard vulnerability is elements at risk, whose vulnerability is a composite with multiple attributes, including physical vulnerability, environmental vulnerability, economic vulnerability, and social vulnerability. To conduct an objective and reasonable geological hazard vulnerability assessment, appropriate indicators should be selected to truly and objectively reflect the basic characteristics of elements at risk in the study area, and the extractability of information should also be considered. Based on the collected data and the attributes of vulnerability of elements at risk, building density and road density were chosen as the evaluation indicators for geological hazard vulnerability in this study, and the evaluation system was constructed. Values were assigned according to the vulnerability index of each indicator, and the final spatial distribution map of geological hazard vulnerability index was obtained through overlay analysis. Geological hazard risk assessment is a pre-assessment of the occurrence of geological hazards and the likelihood of resulting casualties, economic losses, and other damages. Based on a thorough investigation and analysis of various disaster-inducing geological conditions and triggering factors, combined with an evaluation of the magnitude and degree of potential losses (including population and economy) and disaster resistance capacity within the study area, it constitutes a comprehensive assessment of geological hazards. On the basis of disaster-inducing geological analysis, combined with evaluation factors and expert scoring, the 1–9 scale method proposed by Saaty was used to construct the judgment matrix for the study area. Since the correlation between each evaluation factor and landslides and collapses differs respectively, the judgment matrices were constructed separately (Table 4).

Table 3. Classification of Evaluation Factors for Landslide Geological Hazards

No.	Evaluation Factor	Sub-evaluation Factor	Assignment

1	Slope Gradient(°)	＜10	1
2		10-20	2
3		20-30	3
4		＞30	4
5	Aspect	Sunny slope	4
6		Shady slope	2
7		Semi-sunny slope	3
8		No aspect	1
9	Elevation(m)	＜600	1
10		600-700	2
11		700-800	3
12		＞800	4
13	Distance to Structures(m)	＜200	4
14		200-500	3
15		500-1000	2
16		＞1000	1
17	Distance to Drainage(m)	＜200	4
18		200-500	3
19		500-1000	2
20		＞1000	1
21	Distance to Roads(m)	＜200	4
22		200-500	3
23		500-1000	2
24		＞1000	1
25	Stratigraphic Lithology	Upper Permian	1
26		Upper Carboniferous	2
27		Middle–Lower Permian	3
28		Middle–Lower Jurassic	4
29	Vegetation Coverage	＜0.25	4
30		0.25-0.5	3
31		0.5-0.75	2
32		＞0.75	1

Table 4. Information Table of Judgment Matrix for Landslide Susceptibility

Geological hazard	Slope gradient	Aspect	Elevation	Distance to structures	Distance to drainage	Distance to roads	Stratigraphic lithology	Vegetation coverage
Slope gradient	1	2	2	0.5	1	0.5	0.5	0.5
Aspect	0.5	1	2	0.5	1	0.5	0.5	1
Elevation	0.5	0.5	1	0.333	0.5	0.5	0.333	0.5
Distance to structures	2	2	3	1	0.5	0.5	0.5	1
Distance to drainage	1	1	2	3	1	1	0.5	2
Distance to roads	2	2	2	2	1	1	0.5	1
Stratigraphic lithology	2	2	3	2	2	2	1	2
Vegetation coverage	2	1	2	1	0.5	1	0.5	1

(4)Weight Calculation

The eigenvectors of the above judgment matrices, which represent the weight values of each evaluation factor, were calculated using the sum-product method according to the corresponding formula, with detailed results shown in Table 6. The maximum eigenvalue λmax, consistency index CI, and consistency ratio CR of each judgment matrix were computed using the formula, and all judgment matrices established for different geological hazards yielded CR<0.1, indicating satisfactory consistency. The weight results obtained by the Analytic Hierarchy Process (sum-product method) are as follows: slope gradient accounts for 10.147%, aspect for 9.186%, elevation for 5.676%, distance to structures for 12.549%, distance to drainage for 14.045%, distance to roads for 14.879%, stratigraphic lithology for 21.898%, and vegetation coverage for 11.62%.

Table 5. Consistency Test Results

Maximum eigenvalue	CI value	RI value	CR value	Consistency test result
8.381	0.054	1.404	0.039	Passed

Table 6. Statistical Table of Calculation Results for Eigenvectors of Evaluation Factors

Item	Eigenvector	Weight value(%)	Maximum eigenvalue	CI value
Slope gradient	0.812	10.147		
Aspect	0.735	9.186	8.381	0.054
Elevation	0.454	5.676		

Distance to structures	1.004	12.549
Distance to drainage	1.124	14.045
Distance to roads	1.19	14.879
Stratigraphic lithology	1.752	21.898
Vegetation coverage	0.93	11.62

3. Results

3.1 Susceptibility Assessment

By overlaying the susceptibility index raster layers of each evaluation factor (Fig. 2), landslide susceptibility in the area was classified into four grades: high, moderate, low, and non-susceptible, thus obtaining the regional geological hazard susceptibility assessment map of the Libo section (Fig. 3). The non-susceptible area of geological hazards in the Libo–Huanjiang heritage site is 237.73 km², accounting for 29.20% of the total area; the low-susceptible area is 349.54 km², accounting for 42.94%; the moderate-susceptible area is 166.35 km², accounting for 20.43%; and the high-susceptible area is 60.44 km², accounting for 7.42%, which is mainly distributed in the western part of the study area.

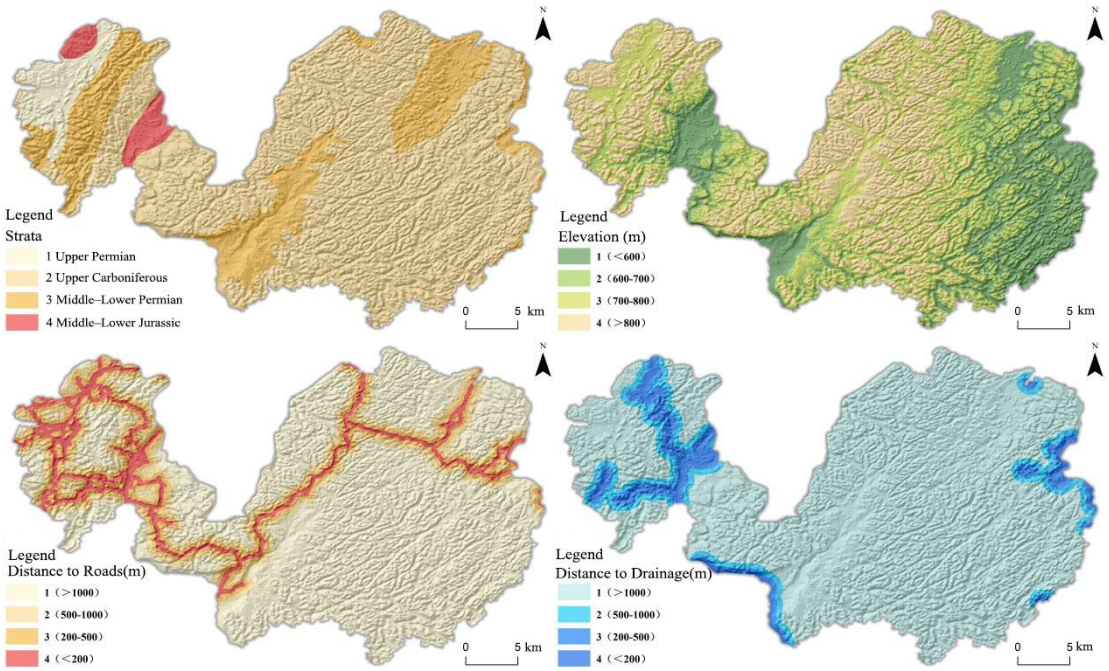

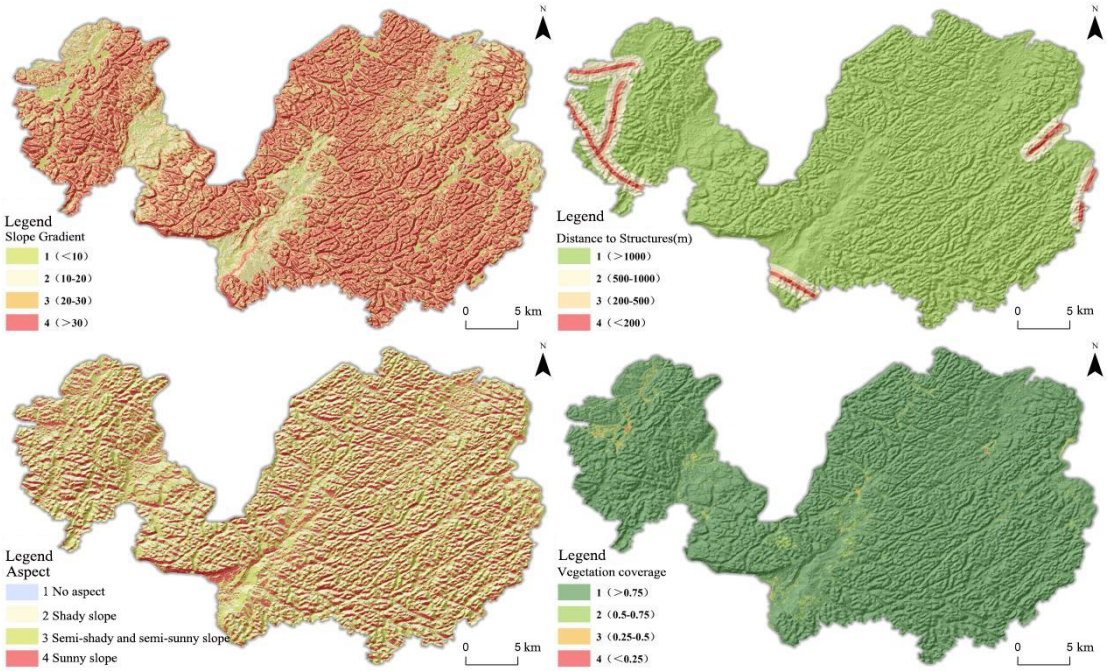

Figure 2. Distribution Map of Evaluation Factors for Geological Hazard Susceptibility

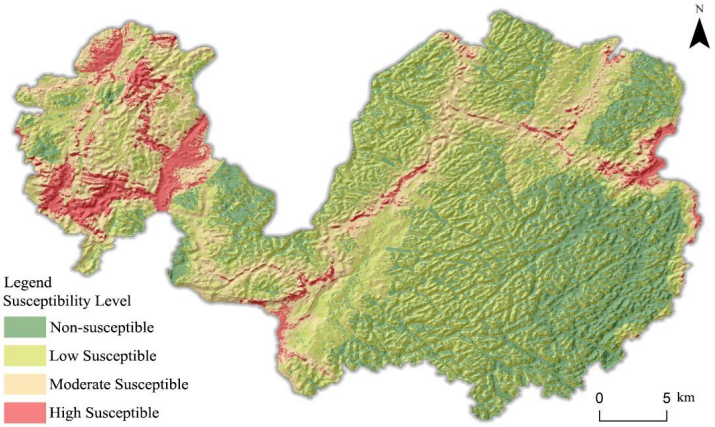

Figure 3. Raster Map of Geological Hazard Susceptibility Assessment

3.2 Hazard Assessment Results

Using the above hazard calculation method, the hazard index was classified into four hazard levels (very high, high, moderate, and low) by the natural breaks classification method in ArcGIS, as shown in Figure 4. The area of the low-hazard zone for geological hazards in Libo–Huanjiang is 222.60 km², accounting for 27.34% of the total area; the moderate-hazard zone is 397.68 km², accounting for 48.85%; the high-hazard zone is 129.65 km², accounting for 15.93%; and the very high-hazard zone is 64.14 km², accounting for 7.88%.

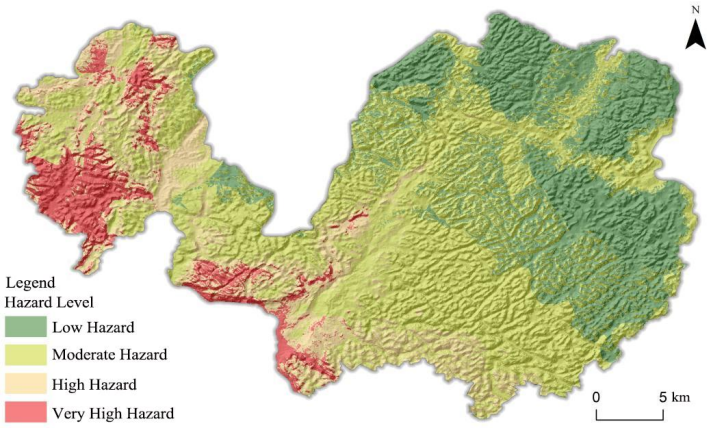

Figure 4. Geological Hazard Assessment Map

3.3 Vulnerability Assessment Results

According to the assignment of vulnerability indices for each vulnerability assessment indicator, the final distribution map of geological hazard vulnerability index was obtained through overlay analysis. The vulnerability index was divided into four levels: very high, high, moderate, and low, as shown in Figure 5. The area of low vulnerability to geological hazards in the Libo-Huanjiang Heritage Site is 663.15 km², accounting for 81.46% of the total area; the moderate vulnerability area is 95.41 km², accounting for 11.72%; the high vulnerability area is 46.56 km², accounting for 5.72%; and the very high vulnerability area is 8.95 km², accounting for 1.10%, which is mainly distributed in the western part of the study area.

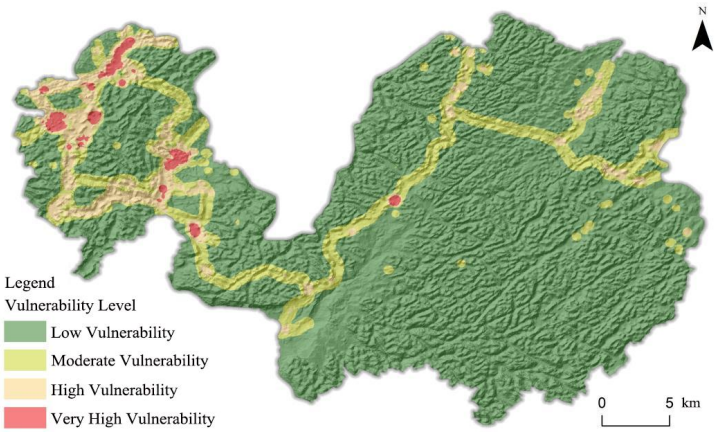

Figure 5. Geological Hazard Vulnerability Assessment Map

3.4 Risk Assessment Results

The county-level geological hazard risk index distribution map (Fig. 6) was obtained by calculating the geological hazard risk index as the product of the geological hazard hazard index and the vulnerability index. According to the magnitude of the risk index, the survey area was divided into four risk levels (very high, high, moderate, and low) using the natural breaks method. Under normal working conditions, the area of the low-risk zone for geological hazards in Libo–Huanjiang is 555.91 km²,

accounting for 68.29% of the total area; the moderate-risk zone is 127.15 km², accounting for 15.62%; the high-risk zone is 112.10 km², accounting for 13.77%; and the very high-risk zone is 18.91 km², accounting for 2.32%, which is sporadically distributed in the northwestern part of the study area.

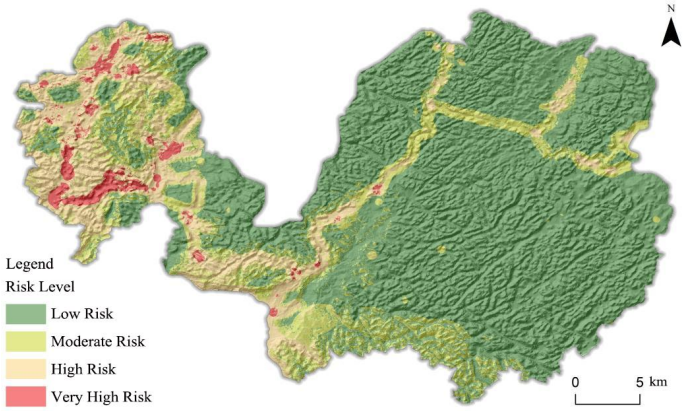

Figure 6. Geological Hazard Risk Assessment Map

4. Discussion

4.1 Spatial Differentiation and Genetic Analysis of Risk Levels

The geological hazard risk in the Libo–Huanjiang Heritage Site presents a remarkable spatial differentiation characteristic of high local concentration and overall dominance of low risk, which is highly consistent with the spatial matching of the regional geological environment background, inducing factors and the intensity of human activities. In terms of the composition of risk levels, low-risk areas account for 68.29%, while very high-risk areas account for only 2.32% and are sporadically distributed in the northwest. This pattern is essentially determined by the three-dimensional synergistic effect of stability of the disaster-forming environment, disaster-inducing intensity and exposure degree of hazard-affected bodies.

The high-susceptibility zone (7.42%) and high-vulnerability zone (5.72%) are both mainly concentrated in the western part of the study area, and show a high spatial overlap with the very high-hazard zone (7.88%), forming a high-value coupling zone of susceptibility-hazard-vulnerability. This region is exactly the core affected zone of the Libo Maolan Fault. The strata are dominated by carbonate rocks with low shear strength, combined with topographic conditions where slopes exceed 25°, which constitutes the innate geological basis for disaster formation. Meanwhile, the western part features dense tourist roads, frequent visitor activities, and high building and road density, which increase the vulnerability of hazard-affected bodies. Frequent triggering by extreme rainfall further amplifies the hazard level, eventually forming a high-risk agglomeration effect. In contrast, the central and eastern parts of the study area are dominated by low-to-non-susceptible zones and low-vulnerability zones (81.46%). This area is far from fault structures, with gentle terrain slopes, high vegetation coverage, weak human disturbance, and strong geological environment stability. Both the disaster-triggering probability and loss potential are low, forming a safe core zone for heritage

protection.

Very high-risk zones are only sporadically distributed in the northwestern part, which reflects the extreme coupling scenario of "strong disaster-forming environment + high triggering probability + high vulnerability". As the transition zone between the Yangtze Paraplatform and the South China Fold Belt, the northwestern part shows more intensive development of faults and karst, with a high degree of rock and soil fragmentation. Meanwhile, a small number of residential areas and tourist trails are distributed in this region. The exposure of hazard-affected bodies highlights the potential of disaster losses, and the additional triggering effect of extreme rainfall eventually gives rise to local very high-risk points.

4.2 Synergistic Mechanism of Evaluation Dimensions

The formation of geological hazard risk is the result of nonlinear coupling among susceptibility, hazard and vulnerability. The assessment results of the Libo–Huanjiang Heritage Site clearly reveal the synergistic law of the three factors. In terms of the hierarchical composition of each dimension, susceptibility is dominated by low-to-non-susceptible zones, hazard is dominated by moderate-to-low hazard zones, and vulnerability shows an extremely low-level characteristic. This low-vulnerability-dominated pattern significantly reduces the overall risk level, resulting in low-risk areas accounting for 68.29%.

The correlation between hazard and susceptibility is particularly prominent: the spatial overlap between high-susceptibility zones and high-to-very-high hazard zones coincides exactly with the areas affected by heavy rainfall during the concentrated rainfall period. This confirms the disaster-forming logic that "susceptibility is the foundation, and triggering factors are the driving force" — geologically vulnerable areas, when triggered by extreme rainfall, experience a significant increase in disaster probability, promoting the transformation from high susceptibility to high hazard. The regulatory effect of vulnerability on risk is equally critical. Although some areas exhibit high hazard, the low density of hazard-affected bodies and favorable ecological background across most regions keep vulnerability at a low level. As a result, high hazard cannot be fully converted into high risk, and only local high-risk zones form in the western part where hazard-affected bodies are concentrated. This reflects the weakening effect of ecological buffering on risk in the heritage site.

In addition, an obvious "threshold effect" exists in the hierarchical transformation of each dimension. When the susceptibility index reaches a high level, the annual rainfall exceeds 1600 mm, and the density of buildings and roads surpasses a specific threshold, the synergistic effect of the three factors leads to a leapfrog rise in the risk level, directly jumping from low-to-moderate risk to high-to-very-high risk. This threshold feature provides a key basis for the subsequent hierarchical management and control of risks.

4.3 Relationship Between Risk Pattern and Heritage OUV Conservation

The values of the Libo–Huanjiang Heritage Site are embodied in aesthetic values (VII) and geomorphological values (VIII). The results of this assessment are highly consistent with the core demands of heritage value conservation, providing precise spatial guidance for the protection of

heritage values. The western region, where high-susceptibility, high-hazard and high-vulnerability zones are concentrated, is exactly the core distribution area of peak cluster and peak forest karst landforms. Its unique geology and geomorphology constitute the core carrier of aesthetic and geological values. The occurrence of geological hazards will not only damage the integrity of the landforms but also lead to vegetation degradation, thereby weakening the Outstanding Universal Value (OUV) of the heritage.

It is worth noting that the low-risk zones cover the core areas of Maolan National Nature Reserve in Guizhou and Mulun National Nature Reserve in Guangxi. This region preserves the most intact primeval karst forest at the same latitude worldwide, featuring a highly stable ecosystem and a relatively safe geological environment, thus providing a natural barrier for the long-term conservation of heritage values. Although the sporadically distributed very high-risk zones cover only a small area, they have extended into the Daqikong and Xiaoqikong heritage sites. Once geological hazards occur, they may affect the ecosystems and geomorphological landscapes within the heritage sites through a chain effect, posing a potential threat to the integrity of the heritage. Therefore, these zones should be treated as key areas for prevention and control.

5 Conclusions

Taking the Libo–Huanjiang Karst World Heritage Site as the empirical area, this study establishes a refined risk assessment framework for geological hazards centered on the conservation of Outstanding Universal Value (OUV). By integrating technical approaches including the comprehensive index model and analytic hierarchy process (AHP), susceptibility, hazard, vulnerability and risk assessments were systematically conducted, and the core conclusions are as follows:

1) The geological hazard risk in the Libo–Huanjiang Heritage Site shows a spatial pattern of “local concentration, overall low risk”. Under normal working conditions, low-risk zones account for 68.29% of the total area, while very high-risk zones account for only 2.32% and are sporadically distributed in the northwest. High-risk zones (13.77%) are concentrated in the western part with well-developed faults and intensive human activities, providing clear spatial boundaries for differentiated conservation and risk management of the heritage site.

2) The formation of the risk pattern is dominated by the synergistic effect of susceptibility, hazard and vulnerability: susceptibility is dominated by low-to-non-susceptible zones (72.14%), hazard is dominated by moderate-to-low hazard zones (76.19%), and vulnerability shows an “extremely low-level” characteristic (low-vulnerability zones account for 81.46%). The high-value coupling zones of the three factors lead to local high-risk areas, while the low-vulnerability-dominated pattern significantly reduces the overall risk level.

3) The risk pattern is highly correlated with heritage value conservation: low-risk zones cover most parts of the heritage site, providing a safety guarantee for the long-term conservation of heritage values. High-to-very-high risk zones are concentrated in the western geomorphic heritage areas and human

activity zones, where geological hazards not only threaten human settlement safety but also pose potential risks to the geomorphological integrity and ecosystem stability of the heritage site, making them key prevention and control zones for heritage value conservation.

The integrated method adopted in this study — multi-factor raster overlay + analytic hierarchy process + natural breaks classification — can accurately characterize the refined risk pattern of geological hazards in karst world heritage sites, and the assessment results are highly consistent with the regional reality, providing an extensible technical paradigm for geological hazard risk assessment in ecologically fragile world heritage sites. This study not only enriches the theoretical and methodological system of geological hazard risk assessment in natural world heritage sites, but also provides operable scientific support for practical management by quantifying the risk pattern, which is of great theoretical value and practical significance for promoting the long-term conservation and sustainable development of heritage sites.

Declaration of Competing Interest

The authors declare that there are no conflicts of interest.References

References

Alamgir, M., Campbell, M. J., Sloan, S., Goosem, M., Clements, G. R., Mahmoud, M. I., & Laurance, W. F. (2017). *Economic, Socio-Political and Environmental Risks of Road Development in the Tropics. Current Biology*, *27*(20), 1130-1140.

Allan, J. R., Venter, O., Maxwell, S., Bertzky, B., Jones, K., Shi, Y., & Watson, J. E. M. (2017). Recent increases in human pressure and forest loss threaten many Natural World Heritage Sites. *Biol. Conserv*, *206*, 47-55.

Allan et al. (2017). Recent increases in human pressure and forest loss threaten many Natural World Heritage Sites. *BIOLOGICAL CONSERVATION.*

Beza, B. B. (2010). The aesthetic value of a mountain landscape: A study of the Mt. Everest Trek. *Landscape and Urban Planning*, *97*(4), 306-317.

Birkmann, J., Cardona, O. D., Carreño, M. L., Barbat, A. H., Pelling, M., Schneiderbauer, S., Kienberger, S., Keiler, M., Alexander, D., Zeil, P., & Welle, T. (2013). Framing vulnerability, risk and societal responses: The MOVE framework. *Natural Hazards*, *67*(2), 193-211.

CHAE et al. (2017). Landslide prediction, monitoring and early warning: A concise review of state-of-the-art. *Geosciences Journal*, *21*(6), 1033-1070.

Chen, T. B. (2012). The rescue, conservation, and restoration of heritage sites in the ethnic minority areas ravaged by the Wenchuan earthquake. *Frontiers of Architectural Research*, *1*(1), 77-85.

CHENG et al. (2024). A critical analysis of geological hazard risk assessment including future perspectives. *Sustainability*, *2024*(9), 3701-3721

Cheung, N. K.-W. (2007). At Risk: Natural Hazards, People's Vulnerability and Disasters - by Ben

Wisner, Piers Blaikie, Terry Cannon, and Ian Davis. *The Geographical Journal*, *173*(2), 189-190.

Du, X. S. H., & Wang, Z. G. (2018). Optimizing monitoring locations using a combination of GIS and fuzzy multi criteria decision analysis, a case study from the Tomur World Natural Heritage site. *Journal for Nature Conservation*, *43*, 67-74.

Hagenlocher, M., Renaud, F. G., Haas, S., & Sebesvari, Z. (2018). Vulnerability and risk of deltaic social-ecological systems exposed to multiple hazards. *Science of The Total Environment*, 631-632, 71-80.

Han, F., Yang, Z. P., Liu, X. L., & Di, F. (2011). Impact assessment and protection of outstanding landscape integrity in a natural heritage site: Fairy valley, Kanas Nature Reserve, China. *Journal of Mountain Science*, *8*(1), 46-52.

Klimeš, J. (2013). Landslide temporal analysis and susceptibility assessment as bases for landslide mitigation, Machu Picchu, Peru. *Environmental Earth Sciences*, *70*(2), 913-925.

Ma, X., Lu, Z., & Lin, T. (2010). Ecological risk assessment of Yancheng Coastal Wetland. M*ar. Environ. Sci*, *29*, 599-602.

Morin, C. W. (2015). Visualizations of mosquito risk: A political ecology approach to understanding the territorialization of hazard control. *Landscape and Urban Planning*, *142*, 159-169.

Nicu, I. C., & Romanescu, G. (2016). Effect of natural risk factors upon the evolution of Chalcolithic human settlements in Northeastern Romania (Valea Oii watershed). From ancient times dynamics to present days degradation. *Z. Fur Geomorphol*, *60*, 1-9.

Okeefe, P., Westgate, K., & Wisner, B. (1976). TAKING NATURALNESS OUT OF NATURAL DISASTERS. *Nature*, *260*(5552), 566-567.

Pan, J., & Liu, X. (2016). Landscape ecological risk assessment and landscape security pattern optimization in Shule River Basin. *Chin. J. Ecol*, *35*, 791-799.

Parisi, F., & Augenti, N. (2013). Earthquake damages to cultural heritage constructions and simplified assessment of artworks. *Engineering Failure Analysis*, *34*, 735-760.

Pavlova, I., Makarigakis, A., Depret, T., & Jomelli, V. (2017). Global overview of the geological hazard exposure and disaster risk awareness at world heritage sites. *Journal of Cultural Heritage*, *28*, 151-157.

Serveiss, V. B. (2002). Applying Ecological Risk Principles to Watershed Assessment and Management. *Environmental Management*, *29*(2), 145-154.

SHU et al. (2024). Geological hazard risk assessment and rural settlement site selection using GIS and random forest algorithm. *Ecological Indicators*, *2024*(4), 120-166.

Steen, R. J. C. A. et al. (1999). Ecological risk assessment of agrochemicals in European estuaries. *Environmental Toxicology and Chemistry*, *18*(7), 1574-1581.

Vašíčková, J., Hvězdová, M., Kosubová, P., & Hofman, J. (2019). Ecological risk assessment of pesticide residues in arable soils of the Czech Republic. *Chemosphere*, *216*, 479-487.

Wang et al. (2018). Site selection for municipal solid waste landfill considering environmental health

risks. *Resources, Conservation and Recycling*, *138*, 40-46.

Wang, Y., Yao, S., & Deng, Y. (2019). Spatio-temporal pattern evolution and influencing factors of governance efficiency of soil and water loss in theWeihe River Catchment. *Sci. Geogr. Sin*, *39*, 836-846.

Wang, Z. G., Yang, Z. P., & Du, X. S. H. (2014). Analysis on the threats and spatiotemporal distribution pattern of security in World Natural Heritage Sites. *Environmental Monitoring and Assessment*, *187*(1), 4143.

WARD et al. (2020). Review article: Natural hazard risk assessments at the global scale[J]. Natural *Hazards and Earth System Sciences*, *20*(4), 1069-1096.

Wu, Y., & Deng, N. (2019). Resource-based urban ecological security early warning based on RBF Neural Network Model: A case study of Yulin city. *Ecol. Econ*, *35*, 111-118.

Xu, W., Yang, Y., Zhang, L., Xiao, Y., Wang, X., & Ouyang, Z. (2017). Evaluation methods and case study of regionalecological carrying capacity for early-warning. *Prog. Geogr*, *36*, 306-312.

Xu, W., Yang, Y., Zhang, L., Xiao, Y., Wang, X., & Ouyang, Z. Evaluation methods and case study of regionalecological carrying capacity for early-warning. *Prog. Geogr*, *36*, 306-312.

Yanes, A., Botero, C. M., Arrizabalaga, M., & Vásquez, J. G. (2018). Methodological proposal for ecological risk assessment of the coastal zone of Antioquia, Colombia. *Ecological Engineering*.

Yang, Z. P., Zhang, X. L., Di, F., Wall, G., Liu, X. L., & Shao, R. (2010). Natural heritage values and comparative analyses of Kanas, China. *Journal of arid land*, *2*(3), 197-206.

You, W.-B., He, D.-J., Qin, D.-H., Ji, Z.-R., Wu, L.-Y., Yu, J.-A., Chen, B.-R., & Tan, Y. (2014). System construction of early warning for ecological security at cultural and natural heritage mixed sites and its application: A case study of Wuyishan Scenery District. *Ying Yong Sheng Tai Xue Bao*, *25*, 1455-1467.

Zhang, J., Xiong, K., & Liu, X. C. D. (2023). Exploring the synergy between Karst World Heritage site's OUV conservation and buffer zone's tourism industry development: A case study of the Libo-Huanjiang Karst. *heritage science*, *11*(1).

Zhang, M., Xiong, K., Wang, X. et al. (2022). Natural Beauty and Esthetic Value of Natural World Heritage Sites: A Literature Review and Implications for Karst Geoheritage Sites. *Geoheritage*, *14*(3), 1-13.